Entinostat Prevents Leukemia Maintenance in a Collaborating Oncogene-Dependent Model of Cytogenetically Normal Acute Myeloid Leukemia

STEM CELLS®

TRANSLATIONAL AND CLINICAL RESEARCH

Entinostat Prevents Leukemia Maintenance in a Collaborating Oncogene-Dependent Model of Cytogenetically Normal Acute Myeloid Leukemia

JOANNE M. RAMSEY,[a] LAURA M.J. KETTYLE,[a] DANIEL J. SHARPE,[a] NUALA M. MULGREW,[a] GLENDA J. DICKSON,[a] JANET J. BIJL,[b] PAMELA AUSTIN,[b] NADINE MAYOTTE,[b] SONIA CELLOT,[b] TERENCE R.J. LAPPIN,[a] SHU-DONG ZHANG,[a] KEN I. MILLS,[a] JANA KROSL,[b] GUY SAUVAGEAU,[b,c,d] ALEXANDER THOMPSON[a]

[a]Centre for Cancer Research and Cell Biology, Queen's University Belfast, Northern Ireland, United Kingdom; [b]Institute for Research in Immunology and Cancer (IRIC), University of Montreal, Montreal, Quebec, Canada; [c]Division of Hematology and Research Center, Maisonneuve-Rosemont Hospital, Montreal, Quebec, Canada; [d]University of Montreal, Faculty of Medicine, Montreal, Quebec, Canada

Key Words. Cytogenetically normal acute myeloid leukemia model • Histone deacetylase inhibitor • Connectivity Map • HOXA9-MEIS1 • Entinostat • Therapeutic

ABSTRACT

The incidence of refractory acute myeloid leukemia (AML) is on the increase due in part to an aging population that fails to respond to traditional therapies. High throughput genomic analysis promises better diagnosis, prognosis, and therapeutic intervention based on improved patient stratification. Relevant preclinical models are urgently required to advance drug development in this area. The collaborating oncogenes, *HOXA9* and *MEIS1*, are frequently co-overexpressed in cytogenetically normal AML (CN-AML), and a conditional transplantation mouse model was developed that demonstrated oncogene dependency and expression levels comparable to CN-AML patients. Integration of gene signatures obtained from the mouse model and a cohort of CN-AML patients using statistically significant connectivity map analysis identified Entinostat as a drug with the potential to alter the leukemic condition toward the normal state. Ex vivo treatment of leukemic cells, but not age-matched normal bone marrow controls, with Entinostat validated the gene signature and resulted in reduced viability in liquid culture, impaired colony formation, and loss of the leukemia initiating cell. Furthermore, in vivo treatment with Entinostat resulted in prolonged survival of leukemic mice. This study demonstrates that the HDAC inhibitor Entinostat inhibits disease maintenance and prolongs survival in a clinically relevant murine model of cytogenetically normal AML. STEM CELLS *2013;31:1434–1445*

Disclosure of potential conflicts of interest is found at the end of this article.

INTRODUCTION

Large-scale analysis of the leukemic genome and transcriptome has unearthed abnormalities in key cellular and molecular pathways. Microarray-based gene expression profiling, in particular, has identified novel disease subclasses at diagnosis [1–5]. The ability to sequence complete genomes at high resolution has resulted in the generation of disease-specific data silos. However, the true value of such technologies to the fundamental understanding of the disease state and integration into clinical practice has yet to be fully realized [6]. Connectivity mapping (cMap) is an experimental bioinformatics approach to identify and map underlying genetic differences in disease states to toxicology profiles of small-molecule therapeutics [7]. A recent adaptation of this method that incorporates a robust statistical significance and perturbation algorithm, termed statistically significant connectivity map (sscMap), provides a platform to interrogate relevant models of disease and integrate expression profiling with treatment response to rationally designed therapeutics for redeployment [8, 9].

Several leukemia-associated gene rearrangements have been recapitulated in genetically engineered mouse models, some of which have been used successfully to monitor response to therapy and provide insights into chemosensitivity and chemoresistance [10]. Similarly, transduction/transplantation studies have been widely used to recapitulate deregulated oncogene expression in the leukemia setting and provide a

Author contributions: J.R. L.K., D.S., N.M., G. D., and P.A.: collection and/or assembly of data; J.B.: collection and/or assembly of data and final approval of manuscript, N.M.: provision of study material or patients; S.C.: data analysis and interpretation; T.L.: financial support and final approval of manuscript; S.Z.: data analysis and interpretation, K.I.M.: data analysis and interpretation and final approval of manuscript; J.K.: provision of study material or patients and manuscript writing; G.S.: conception and design and manuscript writing; A.T.: conception and design, collection and/or assembly of data, data analysis and interpretation, and manuscript writing.

Correspondence: Alexander Thompson, Ph.D., Centre for Cancer Research and Cell Biology, Queen's University Belfast, 97 Lisburn Road, Belfast, Northern Ireland BT9 7BL, United Kingdom. Telephone: +44 (0) 28 9097 2927; Fax: +44 (0) 28 9097 2776; e-mail: alex.thompson@qub.ac.uk Received March 3, 2012; accepted for publication March 14, 2013; first published online in STEM CELLS *EXPRESS* April 17, 2013. 1066-5099/2013/$30.00/0 doi: 10.1002/stem.1398

basis for functional studies. The relatively long disease latencies observed in some models, for example, Mixed-Lineage Leukemia-Eleven Nineteen Leukemia (MLL-ENL) and AML1 suggest the need for additional genetic interactions to obtain robust transplantable models more amenable to therapy-related studies [11, 12]. Transduction and transplantation of hematopoietic stem/progenitor cells with combined oncogenic components such as BCR/ABL and AML1, into syngeneic recipients, results in aggressive and transplantable leukemia [13].

Homeodomain (HD) containing proteins regulate developmental processes including hematopoiesis. A subset with an atypical HD defined by a three-amino-loop-extension motif (TALE) form complexes with proteins encoded by the clustered class I *homeobox* (*HOX*) genes. An established body of evidence supports a role for HOX and TALE proteins in leukemogenesis (reviewed by Argiropoulos and Humphries [14]). In particular, altered expression of *HOXA9* has been observed in a significant proportion of both human acute myeloid leukemia (AML) and acute lymphoid leukemia (ALL) and reported as the most consistent indicator of poor prognosis in refractory AML [15–17]. The frequent co-overexpression of *HOXA9* and *MEIS1*, particularly in leukemias harboring MLL-rearrangements [18, 19], suggests a vital genetic interaction between the cofactors, which may be required for leukemia maintenance in a context-dependent manner [20–23]. Notably, expression of *HOXA9* and *MEIS1* is also associated with cytogenetically normal AML (CN-AML) where no major genetic aberrations have been identified [24]. Direct co-overexpression of *HOXA9* and *MEIS1* results in an aggressive, transplantable, and tractable myeloid leukemia in mouse models with a cytogenetically normal genetic background [25].

A conditional *loxP-HOXA9-ires-MEIS1-loxP* mouse model of leukemia (A9M-L2) phenotypically comparable to similar reported models [26] and with levels of the oncogenes comparable to CN-AML patient samples was developed. Gene signatures obtained from A9M-L2 and CN-AML patient samples were submitted to the sscMap platform to identify potential connections with small molecule inhibitors. Of particular note, three of five of the top candidate small molecule inhibitors identified were identical for the human and mouse conditions. One of these molecules, Entinostat (MS-275, SNDX275) was selected for further study. Treatment of primary leukemic cells with Entinostat resulted in reduced cell viability, impaired colony forming potential, and loss of leukemia maintenance in the murine model. Furthermore, a single treatment of Entinostat to leukemic mice in vivo resulted in extension in survival compared to vehicle treatment.

Together these data support a proof-of-principle that integration of focused gene expression profiling with in silico screening using the sscMap platform enables identification of small molecule inhibitors of leukemia maintenance. In addition the *HOXA9-ires-MEIS1* murine model recapitulates the human CN-AML phenotype at the molecular level and may provide a basis for proof-of-concept studies to predict future therapeutic approaches to treatment of this leukemia subtype.

Materials and Methods

Patient Samples and Data

AML samples were obtained at diagnosis. All studies adhered to the tenets of the Declaration of Helsinki, had ethical committee approval, and all samples were collected with informed consent and anonymized. Mononuclear cells were purified using Ficoll-Paque (GE Healthcare BioSciences AB, Uppsala, Sweden, http://www.gelifesciences.com) gradient centrifugation. Expression profiles were generated from human genome expression arrays (HG-U133A or HG-U133 Plus 2.0: Affymetrix, Santa Clara, CA, http://www.affymetrix.com) for nonleukemic (MILE Class 18, $n = 74$) and intermediate risk (MILE Class 13, $n = 351$) excluding patients with *11q23* abnormalities as classified (NCBI Gene Expression Omnibus Accession number: GSE13204) [27].

Animals

Congenic donor CD45.1$^+$ (C57Bl6/Pep3b or C57Bl/6-Ly5.1) and recipient CD45.2$^+$ (C57Bl/6J) mice were bred and maintained in specific pathogen-free facilities (IRIC or BRU-QUB) under guidelines of both the Canadian Council on Animal Care (CCAC) and UK Animals (Scientific Procedures) Act 1986. Experimental procedures were approved by the Comité de Déontologie de l'Expérimentation sur les Animaux de l'Université de Montréal and the Ethical Review Committee for Animal Research, Queen's University Belfast.

Retroviral Infection and Transplantation of Hematopoietic Cells

The *loxP-HOXA9-ires-MEIS1-loxP-Neo* (A9M-L2) vector was constructed by polymerase chain reaction (PCR) cloning (details available on request), and the construct was subcloned into the XhoI/BamHI site of the murine stem cell proviral vector (*MSCV*). All constructs were verified by DNA sequencing. For *MSCV-Cre-GFP*, the XhoI/MluI fragment (1,031 bp) of *pBluescript-Cre* (kindly provided by Dr. Keith Humphries) was blunt ended and subcloned into the HpaI site of the *MSCV-GFP* vector. Generation of vesicular stomatitis virus-pseudotyped retroviruses, infection of hematopoietic cells, and transplantation into mice were performed as described [28]. Recipient mice were sublethally (650–850 cGy) or lethally (1,300 cGy) irradiated prior to transplantation with bone marrow (BM) or fetal liver (FL) cells isolated at 14.5 dpc. Ex vivo exposure to control GFP or Cre-GFP recombinant retroviruses was limited to 48 hours prior to transplantation.

DNA Analyses

High molecular weight DNA was obtained from hematopoietic tissues, and Southern blot analysis was performed as previously described [29]. The probe used was a SalI and MluI fragment of the *neomycin* gene (852 bp).

Leukemia morphology, Immunophenotype, and Flow Cytometry

Tissue infiltration, morphology, and flow cytometry analyses were performed as described [28]. Allophycocyanin (APC)-conjugated CD11b (BD Pharmingen, San Jose, CA, San Diego, http://www.bdbiosciences.com/index[lowen]us.shtml), Fluorescein isothiocyanate (FITC)-conjugated TER119, Phycoerythrin (PE)-conjugated CD150, and APC-conjugated CD48 (eBiosciences, San Diego, CA) antibodies were used for immunophenotyping. APC-conjugated CD45.1 antibody and PE-conjugated CD45.2 antibody (eBiosciences, http://www.ebioscience.com) were used for repopulation and PE-conjugated CD45.1 antibody (Southern Biotech, Alabama) for homing assays. All data were acquired and analyzed using an LSRII cytometer and FACSDiva 6.1.2 (BD Pharmingen) or FlowJo 7.6.5 software (TreeStar Inc., Ashland, OR, http://www.treestar.com). Tissues were treated with Modified Wright's stain and images were captured at 20× objective. Images were captured using an inverted microscope (CKX41) with attached digital camera (E620) both Olympus, Southend-on-Sea, UK.

Gene Expression Profiling

Total BM was collected by flushing femurs and tibias of age-matched control or A9M-L2 mice, and total RNA was isolated and cDNAs were generated as previously described [30]. For stem cell pluripotency and immune response profiling, cDNA samples were prepared with TaqMan Universal PCR mix and (200 ng/100 μL) loaded into each of the eight ports on the

predesigned 384 well cards of the TaqMan Gene Expression Array. Quantitative reverse transcriptase PCR (qRT-PCR) was performed as per the manufacturer protocol and analyzed using the 7900 HT Sequence Detection System, all ABI (Applied Biosystems, Foster City, CA, Foster City, CA, http://www.appliedbiosystems.com). *18S rRNA* was used as the endogenous control calibrator for subsequent analysis. For analysis by the Biotrove transcription factor panel array, RNA was converted to cDNA with High capacity cDNA RT kit (ABI #4368813) and used at 108 ng/μL of cDNA for 32 cycles of qRT-PCR. Expression data were filtered by Ct confidence [mt]300 and presence or absence of a symmetrical peak in a melting curve analysis. An arbitrary Ct value of 26 was used as the cut-off between expressed and nonexpressed genes. The combined expression of *peptidylprolyl isomerase A* (*Ppia*) and *β-Actin* was used as the endogenous control calibrators for subsequent analysis.

A subset of candidate genes identified from the array platforms were used for validation by individual SYBR Green 1 based qRT-PCR assays. For these assays, the original experimental cDNA was used and validated primer sets were obtained from PrimerBank (http://pga.mgh.harvard.edu/primerbank/) using the relevant gene accession numbers.

Bioinformatics and cMap

Connections between drug-induced gene expression profiles and gene signatures representing the AML disease or normal BM (NBM) state were obtained by sscMap [8] to 1,309 reference profiles obtained from the BROAD Institute cMap database. For the mouse model, a list of all genes with a minimum ± fourfold change in expression between AML and NBM ($n = 5$ per group) were ranked and converted to Affymetrix HG-U133A probeset IDs where possible. Differentially expressed genes were identified using a *t* test. A gene signature with 47 Affymetrix probeset IDs, representing 30 individual genes, returned significant connections to drugs at 1% false discovery rate (FDR = 0.01). For the MILE study, the Affymetrix MAS5 value on the log scale was used as a measure of gene expression level. Class 13 (CN-AML plus fewer than three structural abnormalities, excluding 11q23, $n = 351$) versus Class 18 (nonleukemia and healthy BM, $n = 74$) comparison was carried out using two-sample *t* test to identify significantly differentially expressed genes. Following the same FDR criterion as above, a gene signature with 24 Affymetrix Probeset IDs, representing 21 individual genes, was constructed. The two gene lists were submitted to sscMap for connectivity mapping. A perturbation stability score of robustness was calculated for each significant connection (1 = robust, 0 = weak). Candidate drugs were prioritized, based on combined rational application of the connection, statistical significance and perturbation score.

Ex Vivo Entinostat Treatment

Primary AML samples were rapidly thawed and cultured for up to 72 hours in roswell park memorial institute (RPMI) 10% fetal calf serum (FCS) (Life Technologies, Paisley, U.K. http://www.lifetech.com) containing Entinostat, or the pan-histone deacetylase inhibitor Panobinostat (both Selleckchem, Munich, Germany, http://www.selleckchem.com). To reduce the potential for nonspecific effects, the inhibitors were used at the lowest IC_{50} doses reported to result in effective histone deacetylase (HDAC)-1 and pan-HDAC inhibition, [31, 32] or Dimethyl Sulfoxide (DMSO; vehicle control). Cell viability was quantified by evaluation of ATP levels using CellTiter-Glo (Promega, Madison, WI, http://www.promega.com). Primary A9M-L2 or mouse NBM cells were rapidly thawed and allowed to recover in expansion media, as previously described [26]. Recovered mouse cells or primary AML samples were treated in culture with Entinostat or Panobinostat at the stated concentrations or DMSO (vehicle control, final concentration 0.01%) for 24 hours, then plated in MethoCult GF M3434 media (Stem Cell Technologies, Vancouver, BC, Canada, http://www.stemcell.com) or directly transplanted into irradiated recipient mice at the stated concentration and dosage. Methylcellulose cultures were maintained in a humidified incubator at 37°C with 5% CO_2 for up to 10 days when colony formation, colony counts, and photo images were captured and analyzed. Colony staining with 1 mg/mL *p*-iodonitrotetrazolium violet (INT, Sigma-Aldrich, Gillingham, U.K., http://www.sigmaaldrich.com) for 16 hours enabled visualization of colonies and determination of metabolic activity. Images were captured at the stated magnification using an inverted microscope (CKX41) with attached digital camera (E620) both Olympus. Recipient mice were followed until disease development or up to 80 days at which point necropsy was performed and hematopoietic tissue was examined.

In Vivo Entinostat Treatment of Leukemic Mice

Sublethally irradiated (850 cGy) recipient mice ($CD45.2^+$) were transplanted with A9M-L2-derived BM cells (1×10^6) to regenerate leukemia. After 14 days of transplantation, leukemia harboring mice were treated intravenously with vehicle control or a bolus of Entinostat (30 mg/kg) previously shown to be within the maximal tolerated dose range [33, 34]. Mice were monitored until disease development, necropsied and hematopoietic tissue was examined.

Protein Analysis

Total cell lysates were prepared after incubation of leukemic cells (primary A9M-L2 or A9M cell line) in vehicle (DMSO) or histone deacetylase class I inhibitor (HDACi) containing media at the indicated dosage and time, using an SDS extraction protocol (Cell Signaling Technology, Danvers, MA, http://www.cellsignal.com). Proteins were separated by SDS-PAGE and probed with the following antibodies: caspase 3 (1:1,000; Cell Signaling Technology); $p21^{CIP/WAF}$ (1:200; Santa Cruz Biotechnology, Santa Cruz, CA, http://www.scbt.com); Acetyl-Histone H3 (Lys9; C5B11), Histone H3 (D1H2), Acetyl-Histone H4 (Lys8), Histone H4 (L64C1) (1:1,000; Acetyl-Histone Antibody Sampler Kit #9933, Cell Signaling Technology). Equal loading was assessed using a mouse monoclonal *β*-actin primary antibody (1:5,000; Sigma-Aldrich, St Louis, MO). Blots were developed with a chemiluminescence detection system (Immobilon Western Chemiluminescent horseradish peroxidase (HRP) Substrate; MerkMillipore, Billerica, MA, http://www.millipore.com), exposed to X-ray film (SLS/MOL 7016, Analab, Lisburn, U.K.) for up to 20 minutes, developed, and images were obtained using an Auto-Chemi Imaging system (UVP, Upland, CA). Densitometry was performed using an Auto-Chemi Imaging system (UVP, Upland, CA) and LabWorks software (LabWorks software, Version 4.6, UVP, Upland, CA).

Chromatin Immunoprecipitation and qRT-PCR Analysis

A9M or A9M-L2 cells were cultured at a density of 0.625×10^6 per mL in maintenance media supplemented with 300 nM Entinostat or vehicle control. Cells were crosslinked for 10 minutes at 37°C with 1.5% (w/v) formaldehyde after the appropriate treatment time. Chromatin was isolated, sonicated, and immunoprecipited as per manufacturer protocols using the Acetyl-Histone H4 Immunoprecipitation (ChIP) Assay Kit (Millipore, Billerica, MA). qRT-PCR for ChIP enrichment was as per the manufacturer protocol using SYBR Green PCR mastermix (Roche Diagnostics Limited, West Sussex, U.K., http://www.roche-applied-science.com) and analyzed by the ABI PRISM 7500 system (Applied Biosystems). Control immunoprecipitations were performed by substituting Acetyl-Histone H4 antibody with negative control rabbit immunoglobulins (Dako, Cambridgeshire, U.K., http://www.dako.com). Fold enrichment was determined by normalizing threshold cycle values of ChIP samples against sonicated whole cell DNA extract, set at a value of 1. Primer sequences for the $p21^{CIP/WAF}$ ChIP assays were (5′-TCAAAACGACCTGAATGCCTA-3′ and 5′-GTACAGTTAGAGC TGAGTGAGT-3′). The A9M cell line and A9M-L2 primary leukemia cells were also treated with vehicle (DMSO) or

300 nM Entinostat for 8, 16, or 24 hours. Gene expression was assessed by qRT-PCR using SYBR Green PCR mastermix and $p21^{CIP/WAF}$ primers (5′-CACAGGCACCATGTCCA ATC-3′, 5′-GAA ATCTGTCAGGCTGGTCT-3′).

Statistical Analysis

ANOVA of microarray experiments was implemented using Partek Genomics Suite and ANOVA or Student's *t* tests were performed by GraphPad Prism software (GraphPad software, Version 5.0, LA Jolla, CA) or SPSS software package (IBM, Portsmouth, U.K.).

RESULTS

Generation and Functional Validation of the A9M-L2 CN-AML Model

Retroviral transduction of *HOXA9-ires-MEIS1* (A9M) into BM or FL hematopoietic cells has previously been demonstrated to give rise to aggressive leukemias in mice [26]. To investigate the requirement of these collaborating oncogenes in leukemia maintenance, we exploited the Cre-Lox system to generate a conditional clonal A9M leukemia (A9M-L2). A serial limiting dilution transplantation model was designed (Fig. 1A) and Southern blot analysis of digested genomic DNA from hematopoietic tissue indicated low integration and clonality as demonstrated by a small number of EcoRI digested fragments and equivalent banding patterns in all mice and all tissues (Fig. 1B). The leukemia latency, gross morphology (Fig. 1C), immunophenotype (Fig. 1D; supporting information Fig. S1), and tissue infiltration were consistent with previous studies [26]. Retroviral transduction of the A9M-L2 leukemia cells with Cre-GFP followed by cell sorting, to isolate the transduced ($Cre^{+}GFP^{+}$) cells, resulted in a population of cells (Cre^{hi}/GFP^{hi}) in which the *HOXA9-ires-MEIS1* provirus was deleted (~95%) as determined by Southern blot analysis (Fig. 1E), and a population of cells in which the level of exposure to Cre was reduced (Cre^{lo}/GFP^{lo}) resulting in 50% retention of the transgenes (Fig. 1E; supporting information Fig. S2). The latency of leukemia development in recipients of control GFP^{+} or Cre^{lo}/GFP^{lo} A9M-L2 cells was comparable (30 ± 3 days, Fig. 1F) suggesting that the remaining A9M-L2 cells were sufficient to regenerate leukemia. In contrast, recipients of Cre^{hi}/GFP^{hi} A9M-L2 cells in which the transduced *HOXA9* and *MEIS1* transgenes were effectively deleted, resulting in reduced activity of clonogenic progenitors, altered cell growth and gene expression (supporting information Fig. S2), remained healthy, without any overt signs of disease, during the 150-day observation period (Fig. 1F), indicating that expansion of the leukemic cell population depended on continuous overexpression of *HOXA9* and *MEIS1*.

qRT-PCR analysis demonstrated that the clonal mouse leukemia expressed *HOXA9* and *MEIS1* above the levels determined for either normal nonmanipulated mice or human AML with favorable prognostic outcome, but within the range determined for AML with intermediate or adverse prognosis (supporting information Fig. S3). Therefore, combined low viral titers, in vivo limiting dilution, and clonal selection generated a mouse model of induced leukemia characterized by expression levels of *HOXA9* and *MEIS1* comparable to those detected in primary human leukemias. This represented an appropriate model to search for inhibitors of HOXA9/MEIS1-associated leukemia maintenance and/or expansion.

A9M-L2 Model Is Associated with Reduced Gene Expression

Overexpression of *HOXA9* and *MEIS1* results in an AML phenotype. A focus on the associated biology underlying the disease was taken with respect to quantifying molecular signatures. Since HOX and TALE proteins are transcription factors that work within networks and affect progenitor/stem cell function, the Biotrove transcription factor panel and the ABI TaqMan pluripotent stem cell gene expression array were used to quantify gene expression levels. In addition, a TaqMan immune response array was used to quantify expression levels and contribution of immunoregulatory gene networks to the general AML-associated gene signature. In total, 817 individual qRT-PCR assays were examined in duplicate for biological replicates (up to $n = 5$) from age-matched normal control or A9M-L2 leukemia BM. A stringent fourfold difference in expression (equivalent to $\Delta\Delta Ct = \pm 2$) was used as a cut-off to identify robustly increased or decreased expression of candidate genes. Using this criterion, 14% (114/817) of the genes examined demonstrated differential expression between the normal and leukemic states (supporting information Table S1). Of the differentially expressed genes, 83% (95/114) demonstrated reduced expression and only 17% (19/114) demonstrated increased expression in the leukemic state compared to normal controls (Fig. 2A–2C). A cohort of candidate genes from the array datasets was validated by individual qRT-PCR assays, 87% of which showed similar trends in differential expression (supporting information Fig. S4). Perhaps not surprisingly, *HOXA9* and *MEIS1* showed the most significant fold change in expression in A9M-L2 cells (161- and 248-fold, respectively, p [lt] .05) when compared to NBM, further validating both the model and the array platform approach.

A9M-L2 Candidate Genes Associate with Key Molecular Pathways

Submission of the A9M-L2 signature ($n = 114$ genes) to the gene ontology (GO) platform GOEAST and DAVID databases identified cell proliferation and transcription factor activities among the highest ranking biological processes significantly affected in the mouse model of leukemia development. In addition to transcriptional regulation and immune responses, submission of the gene list to either the DAVID analysis platform (supporting information Table S2a, upper panel) or the GOEAST platform (supporting information Table S3) identified enrichment for genes associated with cell proliferation, activation, and apoptosis. Convincingly, both platforms identified similar subsets of genes including cytokines and chemokines, E2F transcription families, and cluster of differentiation markers as being associated with key processes (supporting information Table S2b). While GOEAST was able to identify similar ontologies to DAVID bioinformatics analysis, it was unable to assess pathway perturbation. The leukemic gene signature was therefore compared to the Kyoto Encyclopedia of Genes and Genomes using the DAVID software database. Key biological pathways involving cytokine signaling and adhesion were significantly enriched within the gene signature, and "Hematopoietic Lineage" and "Pathways in Cancer" were highlighted as major associated processes (supporting information Table S2a, lower panel).

Leukemia Gene Signature sscMap Analysis

To obtain a list of small molecule inhibitors with the potential to affect the leukemic state, differentially expressed gene signatures (supporting information Table S4) from the mouse model ($n = 47$ probesets representing 30 genes) or MILE dataset ($n = 24$ probesets representing 21 genes) were submitted for sscMap

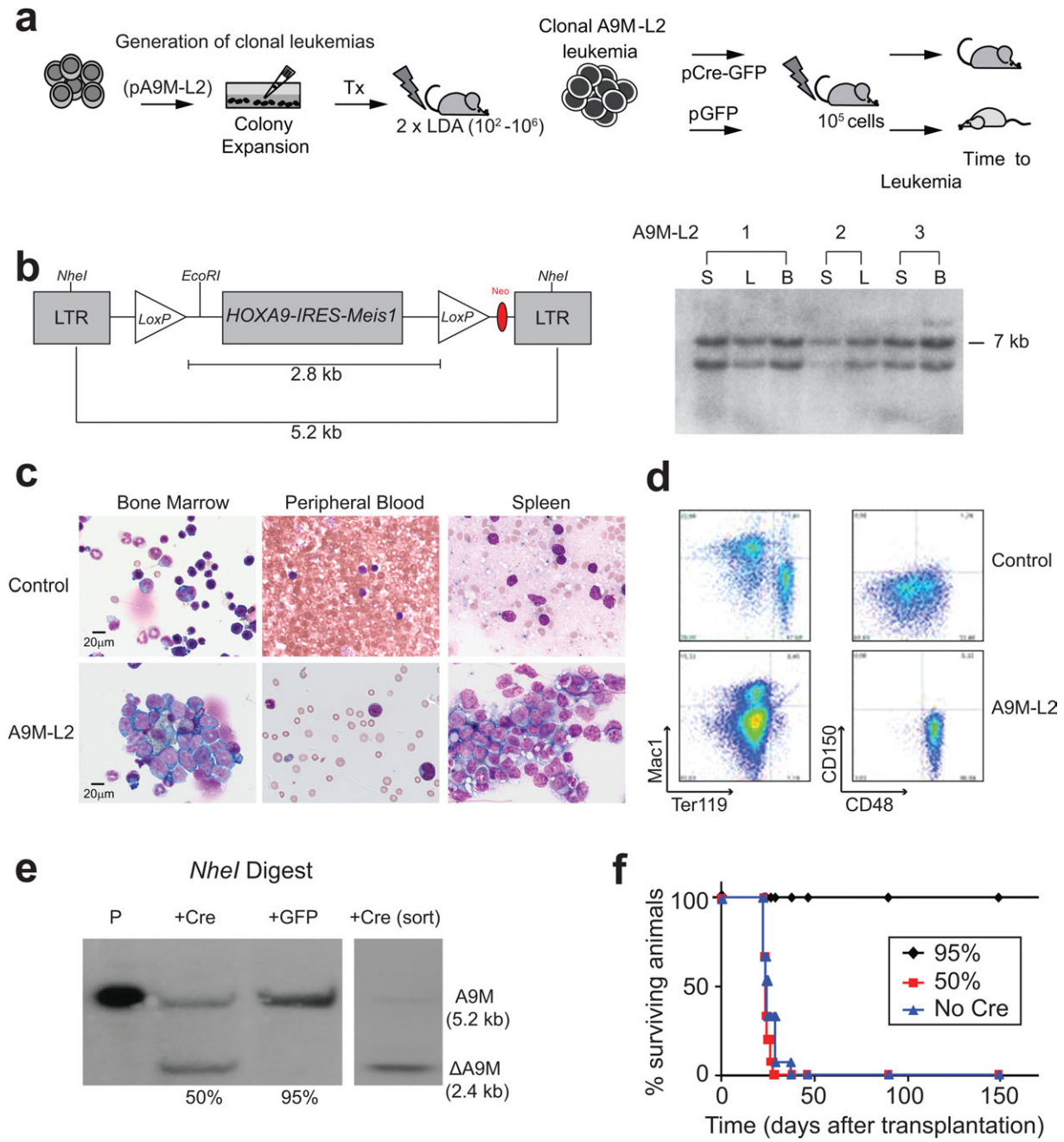

Figure 1. Experimental design and phenotype of conditional leukemia. **(A)**: Schematic representation of the development and experimentation of a conditional *HOXA9-MEIS1* (A9M-L2) mouse model. **(B**, left panel): Structure of the targeting vector used to generate A9M-L2 leukemias indicating the location of flanking loxP sites, the size of anticipated fragments following Cre recombination, and restriction enzymes used to determine integration and clonality. (B, right panel): A representative Southern blot analysis (Neo^R probe) of EcoRI digested genomic DNA obtained from spleen (S), bone marrow (B), or lymph node (L) showing low integration and clonality in three independent A9M-L2 mice. **(C)**: Identification of blast cells in hematopoietic tissues from necropsied A9M-L2 mice compared to age-matched normal controls. **(D)**: Representative dot plots (from $n = 5$) demonstrating levels of surface markers CD11b/Mac-1, CD48, CD150, and Ter-119 analyzed by flow cytometry in both the A9M-L2 model and age-matched normal control bone marrow. **(E)**: Southern blot analysis (Neo^R probe) of NheI digested plasmid (P) or genomic DNA from A9M-L2 mice demonstrating the presence of DNA bands at the sizes expected for successful Cre-recombination of the flanked region at 50% compared to control (pMSCV-GFP) and 95% following selection for GFP^{Hi} populations. **(F)**: Kaplan-Meir plot of the percentage survival of recipient mice receiving either MSCV-GFP treated A9M-L2 cells (No Cre), unsorted MSCV-Cre-GFP treated A9M-L2 cells (50%), or GFP^{Hi} sorted MSCV-Cre-GFP treated A9M-L2 cells (95%); $n = 5$ per group. Abbreviations: B, bone marrow; GFP, green fluorescent protein; LDA, limited dilution assay; LTR, long terminal repeat; S, spleen, L, lymph node; Tx, primary transplant.

analysis. In total 133 of 1,309 and 130 of 1,309 (A9M-L2) connections were shown to be statistically significant, that is, −log10 *p* [mt] 3.15 for the MILE and A9M-L2 datasets, respectively (Fig. 3A). The expected number of false connections = 1 giving an estimated FDR of 0.0075 for the MILE dataset and 0.0077 for the A9M-L2 model dataset, respectively. Application of a perturbation algorithm to the data whereby each gene identified from the normal set (condition 1) versus leukemia set

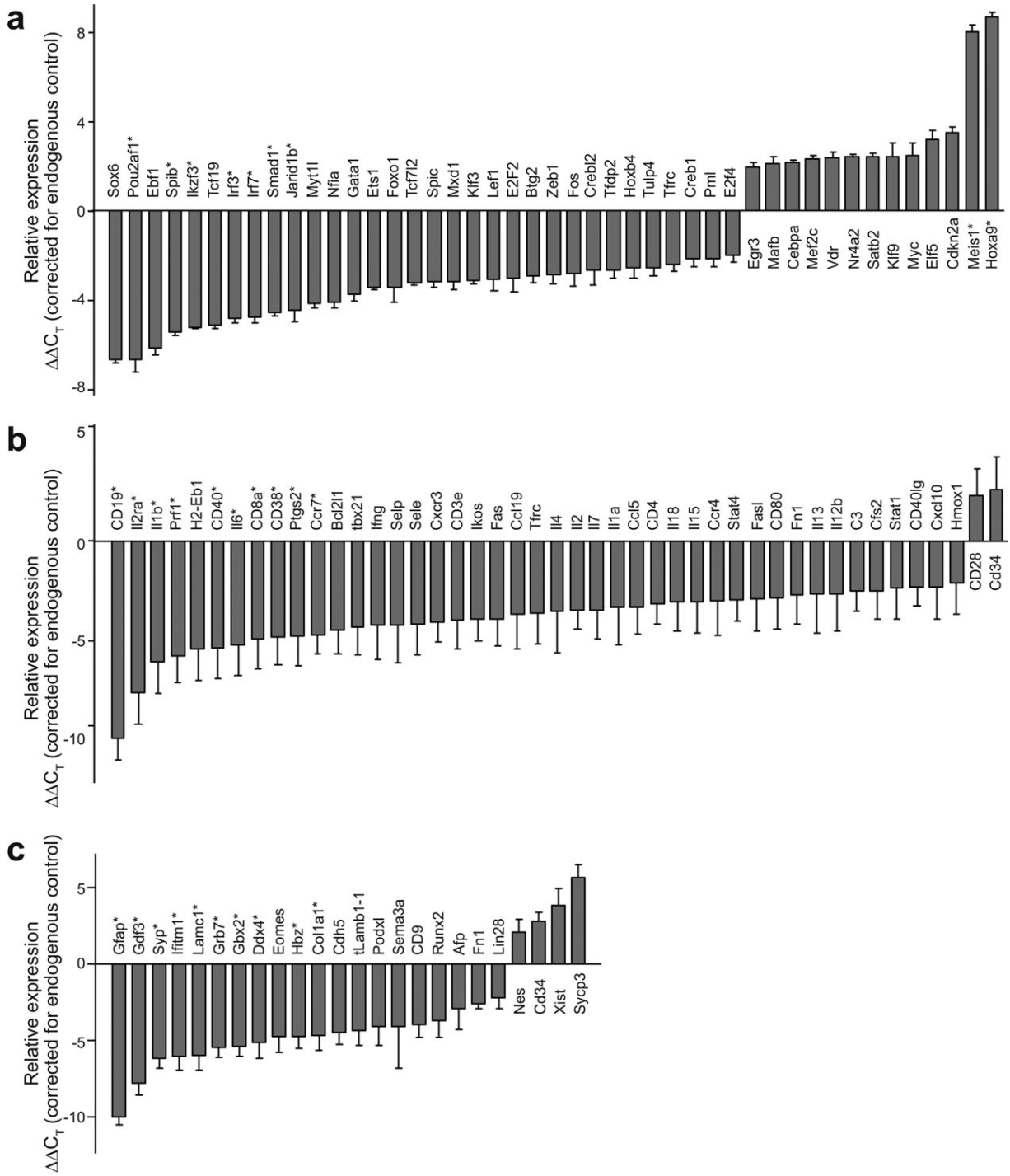

Figure 2. Differential gene expression in A9M-L2 leukemia. Waterfall plots from quantitative reverse transcriptase polymerase chain reaction analysis of an array of genes obtained from bone marrow of A9M-L2 mice compared to age-matched normal bone marrow controls ($n = 5$ per group in duplicate). Relative changes in expression are displayed as $\Delta\Delta C_T$ values corrected for endogenous controls. Only consistent changes in $\Delta\Delta C_T$ values of greater than ± 2 are presented. Mean values $\pm$ S.E.M are plotted from **(A)** stem cell pluripotency, **(B)** immune response, and **(C)** transcription factor array platforms. *A subset of array genes were further validated by individual assays (supporting information Fig. S3).

(condition 2) was individually removed to test the strength of the biological connections resulted in reducing the number of candidate small molecule inhibitors for functional studies (Table 1). A perturbation score of 1 is indicative of an extremely strong connection between a particular drug and the related gene signature, a perturbation score of 0 is indicative of a weak connection.

A shortlist of five potential therapeutics with high normalized connectivity scores (-3.8 to -4.4) and a perturbation score of 1 (p [lt] .00015) was identified from the MILE signature. Similar analysis of the A9M-L2 signature demonstrated connectivity scores of -3.2 to -4.1 (p [lt] .0015). Comparative analysis identified overlap of three candidate drugs from the mouse model and patient samples. Exemestane, a steroidal

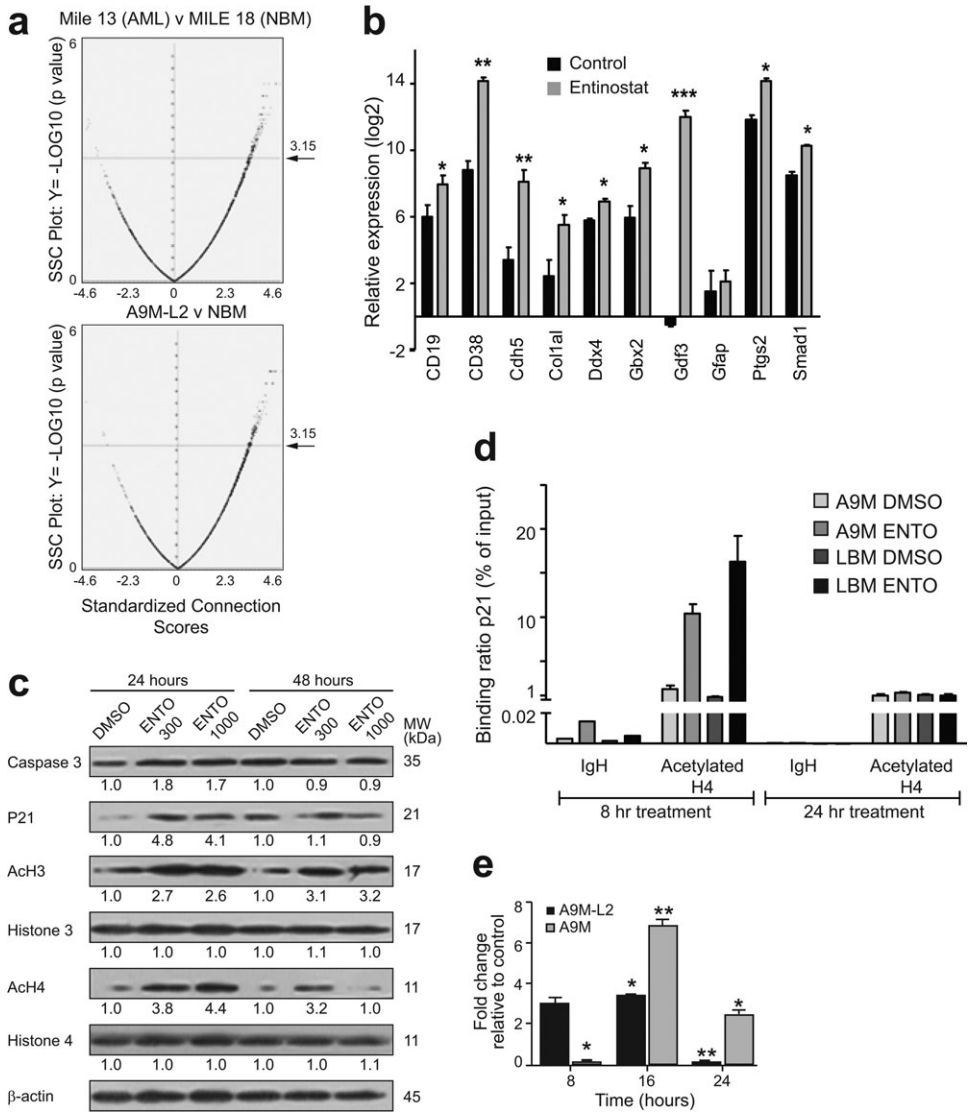

Figure 3. sscMap validation, acetylation of histones, and induction of $p21^{CIP/WAF}$ in Entinostat-treated A9M-L2 cells. **(A)**: A scattergram volcano plot depicting statistically significant connections (SSC) above the 3.15 threshold for –log10 (p value) between 24 MILE data probesets (upper panel) and 47 A9M-L2 data probesets (lower panel). **(B)**: A bar graph of quantitative reverse transcriptase polymerase chain reaction (qRT-PCR) values obtained from A9M-L2 leukemias following short-term treatment (24 hours) with Entinostat (300 nM) or vehicle (DMSO) control ($n = 3$ per group). Relative expression is displayed as $\log_2$ estimated copy number values for *HOXA9* and *MEIS1* (where Ct 35 = 5 copies). A subset of the genelist ($n = 10$) used in the statistically significant connectivity map analysis was examined for differential expression. **(C)**: Western blot and densitometry analysis of A9M cells showing the effect of treatment on levels of proteins implicated in cell survival and activity. Representative data from three independent experiments normalized to β-actin are shown, drug dosages in nM are presented. **(D)**: Bar graph demonstrating a transient increase in AcH4 binding at the $p21^{CIP/WAF}$ promoter following Entinostat treatment of A9M and A9M-L2 primary cells as determined by ChIP-qRT-PCR. **(E)**: A bar graph demonstrating transient upregulation of $p21^{CIP/WAF}$ mRNA expression following Entinostat treatment in A9M and A9M-L2 cells as measured by qRT-PCR analysis. For both (B), (D), and (E) mean values of duplicates ± SEM are plotted ($n = 3$ per group). Significant differences obtained from Student' t tests denoted by *, $p \leq .05$; **, $p \leq .01$; ***, $p \leq .001$. Abbreviations: AML, acute myeloid leukemia; DMSO, Dimethyl Sulfoxide; NBM, normal bone marrow; A9M, HOXA9 plus Meis1 primary cell line; LBM leukemic bone marrow cells from A9M-L2 transplanted mice; ENTO, Entinostat.

aromatase inhibitor, registered a robust perturbation stability of 1 for the MILE but a lower score (0.85) for the A9M-L2 gene signature. Two drugs, namely; TTNPB (tetrahydro-tetramethyl-naphthalenyl-propenyl benzoic acid) and Entinostat had a strong biological connection and perturbation score of 1.0 for both signatures. TTNPB is a retinoic acid agonist shown previously to exhibit in vivo toxicity in mouse [35]. Entinostat, a well-tolerated HDACi [33, 34], was therefore selected as a candidate drug for further analysis. Another HDACi, Panobinostat, not in the 1,309 BROAD Institute cMap Reference Profiles database, was included for comparative analysis.

Validation of sscMap and Entinostat Activity in A9M-L2 Cells

Short-term Entinostat treatment (24 hours) of A9M-L2 cells resulted in increased expression of a subset of genes (9/10), previously identified as being decreased in A9M-L2 cells compared to controls, and part of the signature originally used to obtain the sscMap (Fig. 3B). These data validated the extension of the sscMap from cell lines to the primary leukemia cells. The reported cellular effects of Entinostat, most notably antiproliferative responses, were functionally

Table 1. Candidate small molecule inhibitors (statistically significant connectivity map)

Compound	Replicate	Raw score	*p* value	Normalized score	Sig. mark	Perturbation stability
MILE Study Class 18 NBM ($n=74$) vs. MILE Study Class 13 CN-AML ($n=351$)						
Dinoprostone	4	−0.254	1.00E − 05	−4.359	1	1
Entinostat	2	−0.394	2.00E − 05	−3.871	1	1
Meteneprost	4	−0.251	1.40E − 04	−3.834	1	1
Exemestane	1	−0.448	8.00E − 05	−3.799	1	1
TTNPB	2	−0.376	1.20E − 04	−3.764	1	1
Todralazine	5	0.252	1.00E − 05	4.209	1	1
Dequalinium chloride	4	0.350	1.00E − 05	4.312	1	1
Guaifenesin	6	0.233	1.00E − 05	4.492	1	1
Sulfadiazine	5	0.247		4.515	1	1
Triflusal	3	0.457	1.00E − 05	4.670	1	1
Murine model NBM ($n=5$) vs. A9M-L2 ($n=5$)						
TTNPB	2	−0.295	2.00E − 05	−4.134	1	1
Entinostat	2	−0.275	1.20E − 04	−3.783	1	1
Ampyrone	5	−0.177	7.00E − 04	−3.385	1	0.85
Oligomycin	1	−0.281	8.80E − 04	−3.339	1	0.50
Exemestane	1	−0.267	0.00148	−3.170	1	0.13
Beclometasone	3	0.152	2.00E − 05	4.428	1	1
Sotalol	4	0.185	2.00E − 05	4.428	1	1
Mesalazine	5	0.132	1.00E − 05	4.449	1	1
Levocabastine	4	0.186	1.00E − 05	4.493	1	1
Glafenine	4	0.190	1.00E − 05	4.980	1	1

Abbreviations: CN-AML, cytogenetically normal acute myeloid leukemia; NBM, normal bone marrow.

validated by exposing A9M-L2 cells to the drug for up to 48 hours. This treatment resulted in transient hyperacetylation of Histones H3 and H4 and increased $p21^{CIP/WAF}$ levels. However, no significant decrease in caspase 3 levels or accumulation of cleaved Poly (ADP-ribose) polymerase (PARP) or caspase 3 products could be detected by Western blot analysis (Fig. 3C and data not shown). The transient increase in $p21^{CIP/WAF}$ protein levels following Entinostat treatment was mimicked by a transient increase in AcH4 occupancy at the $p21^{CIP/WAF}$ promoter locus (Fig. 3D) and upregulation of $p21^{CIP/WAF}$ mRNA expression in both A9M and A9M-L2 primary cells (Fig. 3E). The transient effects may be due to low metabolic stability of Entinostat or high background of HDAC activity in A9M leukemic cells.

Three drugs with neutral connectivity scores ([lt] ±0.15) and perturbation values of 0 namely; tamoxifen, thiamine, and ascorbic acid were examined as negative controls for the sscMap analysis. None of the treatments resulted in significant increase in the sscMap gene signature or affected colony formation of A9M-L2 cells (supporting information Fig. S5).

Entinostat Reduces CN-AML Viability and Colony Formation of A9M-L2

Primary CN-AML patient samples ($n = 6$) cultured in Panobinostat (7 nM) or Entinostat (300 nM) for up to 72 hours showed a significant decrease in viability compared to DMSO (vehicle) controls in liquid culture (Fig. 4A). Methylcellulose culture demonstrated reduced clonogenic potential and cellularity of colonies produced from Entinostat-treated primary CN-AML cells compared to Panobinostat or vehicle treated controls (Fig. 4B), even though treatment of A9M-L2 cells with 300 nM Entinostat or 7 nM Panobinostat resulted in comparable increased histone acetylation (supporting information Fig. S6). Entinostat treatment of A9M-L2 primary leukemia cells resulted in a similar marked reduction in clonogenic potential and decreased cellularity compared to Panobinostat, or vehicle and untreated controls, as demonstrated by INT staining (Fig. 4C). The observation that Entinostat treatment did not result in a significant decrease in colony formation of NBM cells (Fig. 4D) suggests the leukemic cells are particularly Entinostat sensitive.

Entinostat Treatment Prevents A9M-L2 Leukemia Maintenance and Extends Survival of Leukemic Mice

The sensitivity of A9M-L2 cells to Entinostat was further demonstrated in parallel transplantation assays. Aliquots of the ex vivo-treated and control A9M-L2 cells used for the colony assays were directly transplanted into recipient mice. A dramatic decrease in the number of leukemia initiating cells in the Entinostat treated cohorts was demonstrated by a complete absence of overt leukemia during the 80-day observation period (Fig. 5A left panel), and no leukemic cell infiltrates (Fig. 5A right panel). In contrast, recipients of untreated, DMSO-treated, or Panobinostat-treated A9M-L2 cells succumbed to leukemia within approximately 32 days after transplantation. Entinostat treatment of NBM cells was well tolerated by recipient mice following transplantation (Fig. 5A left panel) and homing to the spleen or short-term repopulation in spleen and bone marrow were not markedly affected compared to controls (supporting information Figs. S7, S8). Interestingly, both NBM and A9M-L2 cells treated with Entinostat demonstrated a slight reduction in homing to the bone marrow (supporting information Fig. S7), which may warrant further examination. The low dose of HDACis used in the ex vivo model treatments, sufficient to activate $p21^{CIP/WAF}$, did not induce apoptosis as measured by Annexin V/Propidium Iodide staining. This phenomenon was, however, observed when drug concentrations were increased to 1 μM and 25 nM for Entinostat and Panobinastat, respectively (supporting information Fig. S9).

To determine whether Entinostat was capable of suppressing leukemia development in vivo, recipients of A9M-L2 cells were treated with a single bolus of Entinostat or vehicle control on day 14 after leukemia initiation by transplantation and assessed daily for development of AML. Entinostat treatment prolonged the survival time of treated leukemic mice by up to 8 days ($p = .0140$) compared to controls (Fig. 5B left panel), suggesting that in vivo Entinostat treatment noticeably suppressed and delayed expansion of leukemic cell populations.

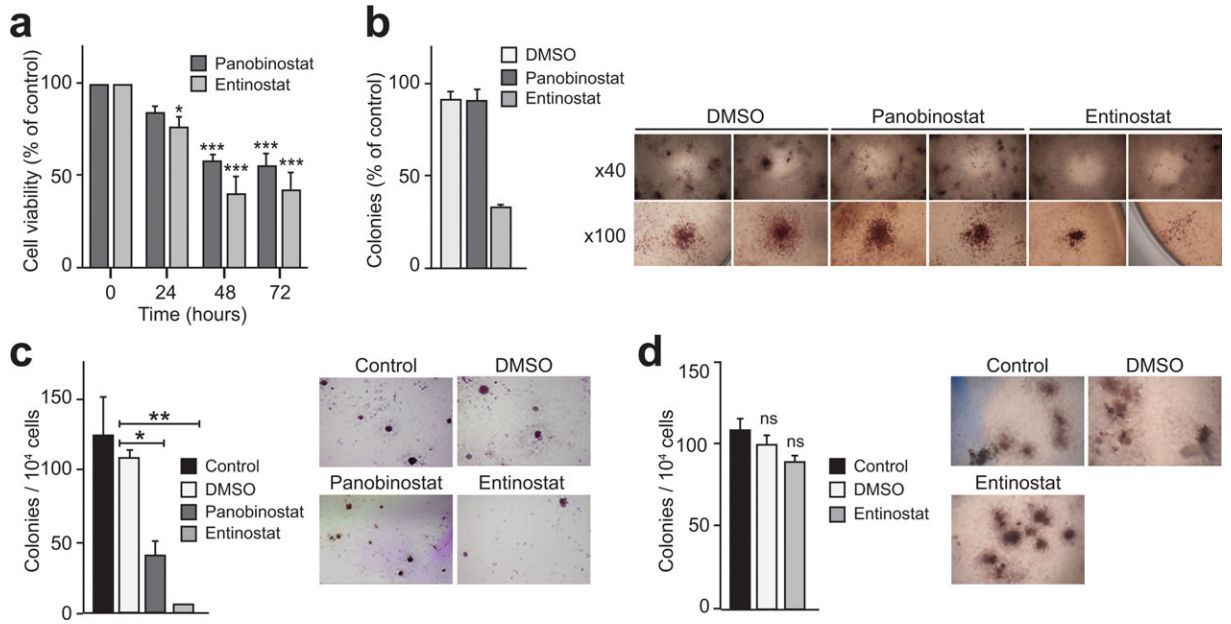

Figure 4. Entinostat reduces cytogenetically normal acute myeloid leukemia (CN-AML) viability and reduces colony formation of A9M-L2 cells. **(A)**: Bar graph demonstrating viability of primary CN-AML samples following Entinostat (300 nM) or Panobinostat (7 nM) treatment ($n = 6$ per group). Cell viability was assessed as relative fluorescence units obtained from the measurement of ATP concentration at the specified time. **(B)**: Representative colony images and the total colony forming cell (CFC) content (lower right panel) of the primary CN-AML cell populations treated with vehicle (DMSO), Panobinostat (7 nM), or Entinostat (300 nM). **(C)**: Colony formation of A9M-L2 cells ($n = 3$ per group) following control, DMSO, Entinostat (300 nM), or Panobinostat (7 nM) treatment. Left panel, total CFC content of the treated cell populations (mean ± SD, $n = 3$, two experiments); right panel, representative images of colonies. **(D)**: Colony formation of normal bone marrow samples ($n = 3$ per group) following control, DMSO, or Entinostat (300 nM) treatment. Left panel, total CFC content (mean ± SD, $n = 3$, two experiments); right panel, representative images of colonies. Asterisks denote significant differences between the treatments and controls (Student's t tests *, $p \leq .05$; ** $p \leq .01$; *** $p \leq .001$). Abbreviation: DMSO, Dimethyl Sulfoxide.

Mice that succumbed to leukemia following the single Entinostat treatment presented with a similar phenotype, including tissue infiltration (Fig. 5B right panel) as vehicle controls.

Discussion

The frequent co-overexpression of *HOXA9* and *MEIS1* in AML, particularly in the absence of an underlying genetic rearrangement, [36, 37] suggests an important role for this axis above and beyond the well-established link with 11q23 translocations (reviewed by Muntean and Hess [38]). Co-overexpression of *HOXA9* and *MEIS1* results in an aggressive and tractable leukemia in mouse which makes it an attractive model for molecular and genetic studies [26]. In this work, we explored the usefulness of a conditional *HOXA9/MEIS1*-dependent mouse model to investigate and challenge leukemia maintenance. A combination of low viral titer and transplantation with limiting numbers of leukemia initiating cells resulted in a robust clonal disease that expressed the collaborating oncogenes at levels representative of CN-AML patient samples. Deletion of the collaborating oncogenes following exposure to *Cre*-recombinase resulted in altered colony and cell growth and loss of leukemia maintenance, defining a potential therapeutic window. However, therapeutic targeted gene deletion is currently far removed from the clinical setting and for that reason a drug redeployment strategy was adopted for candidate drug discovery.

Gene expression analyses of the A9M-L2 leukemia identified reduced expression (below fourfold) of an array of transcription factor, immune responsive and pluripotent stem cell associated genes compared to age-matched normal controls. Only a minor fraction of differentially expressed genes (17%) demonstrated increased expression above fourfold compared to NBM controls. The alteration in gene expression obtained from leukemic bone marrow of A9M-L2 mice reflects the biology of end-stage disease and is thus unlikely to represent direct targets of the collaborating oncogenes. However, some of the genes within the signature, including CD34 and CD28, have been previously identified as potential targets of HOXA9/MEIS1 [39].

GO and pathway analysis of the gene signature obtained from the A9M-L2 model reflected the pathways interrogated by the specific arrays but furthermore identified regulation of proliferation, apoptosis, hematopoietic lineage, and cancer pathways (among others) as key processes associated with the differentially expressed genes. Submission of the CN-AML and A9M-L2 signatures to sscMap analysis identified robust connectivity between five drugs, in both the clinical and mouse model samples, associated with promoting condition 1 (normal bone marrow) over condition 2 (leukemia), thereby indicating therapeutic potential. Furthermore, three of the drugs identified (Entinostat, TTNPB, and Exemestane) showed direct overlap between the CN-AML patients and A9M-L2 model of which two (Entinostat and TTNPB) demonstrated statistically robust perturbation scores of 1. One of the compounds (TTNPB) had previously been shown to have in vivo toxicity in mouse models [35] and, therefore, Entinostat, a HDACi shown to be well-tolerated in vivo [33, 34], was selected for further analysis.

Short-term exposure of A9M-L2 cells to low-dose Entinostat (300 nM) resulted in acetylation of Histones H3 and H4, upregulation of the cell cycle inhibitor $p21^{CIP/WAF}$, and lack of induction of apoptosis in agreement with previous findings [40]. Low-dose Entinostat or Panobinostat treatments significantly decreased cell viability of primary CN-AML cells in

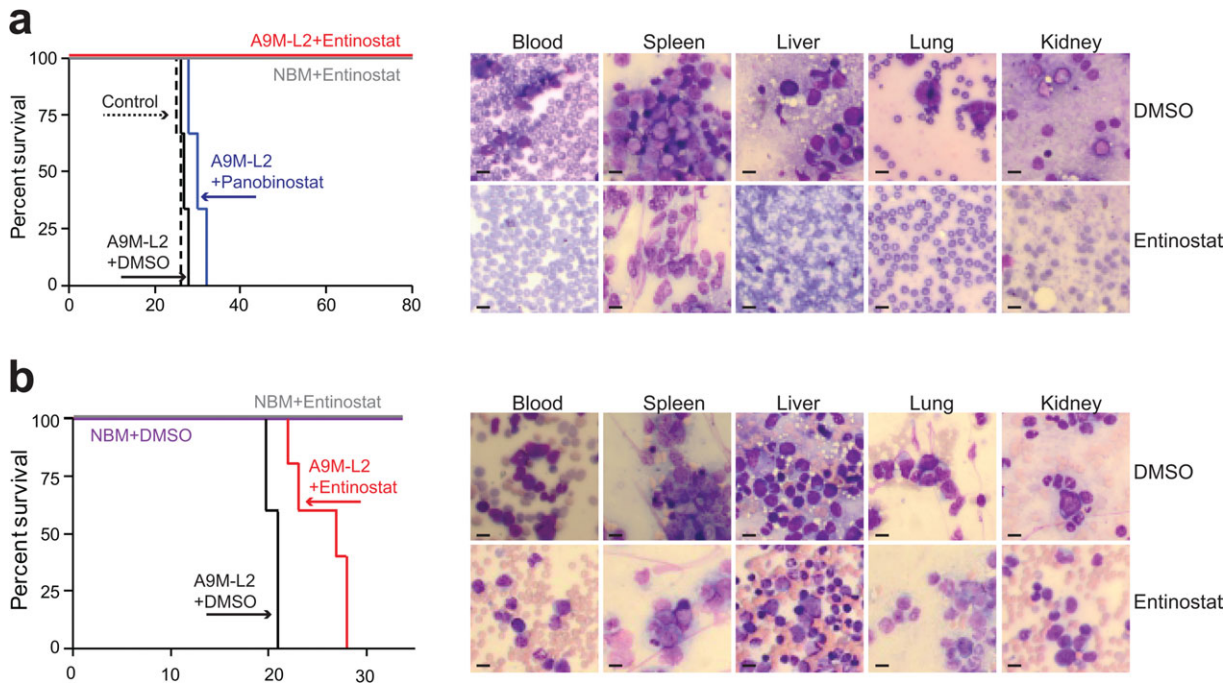

Figure 5. Entinostat treatment prevents A9M-L2 leukemia maintenance and results in prolonged survival in vivo. Kaplan-Meier plots demonstrating correlation between treatment regimens and survival in leukemic mice. (**A**, left panel): A9M-L2 cells were incubated ex vivo for 24 hours in culture with control media, or in media supplemented with vehicle, or Panobinostat (7 nM), or Entinostat (300 nM) then transplanted (5×10^5 cells) into sublethally irradiated (850 cGy) mice, which were closely monitored and sacrificed at the first sign of disease. Normal bone marrow cells treated with Entinostat (300 nM) were transplanted in a control mouse cohort. (A, right panel): Blood smears and tissue touchpreps stained with Wright-Giemsa showing leukemia infiltration of peripheral blood and solid tissues. (**B**, left panel): Kaplan-Meier plots demonstrating prolonged survival in leukemic (A9M-L2) mice, given an i.v. bolus of Entinostat (30 mg/kg) at day 14 following transplantation, compared to DMSO controls ($n = 5$ per group). A control mouse cohort (NBM) was similarly treated and demonstrated no morbidity within the observation time frame. Significant difference between the treatment and control (Log-rank Mantel-Cox Test; p value = .014). Scale bars = 20 μM. Abbreviations: DMSO, Dimethyl Sulfoxide; NBM, normal bone marrow.

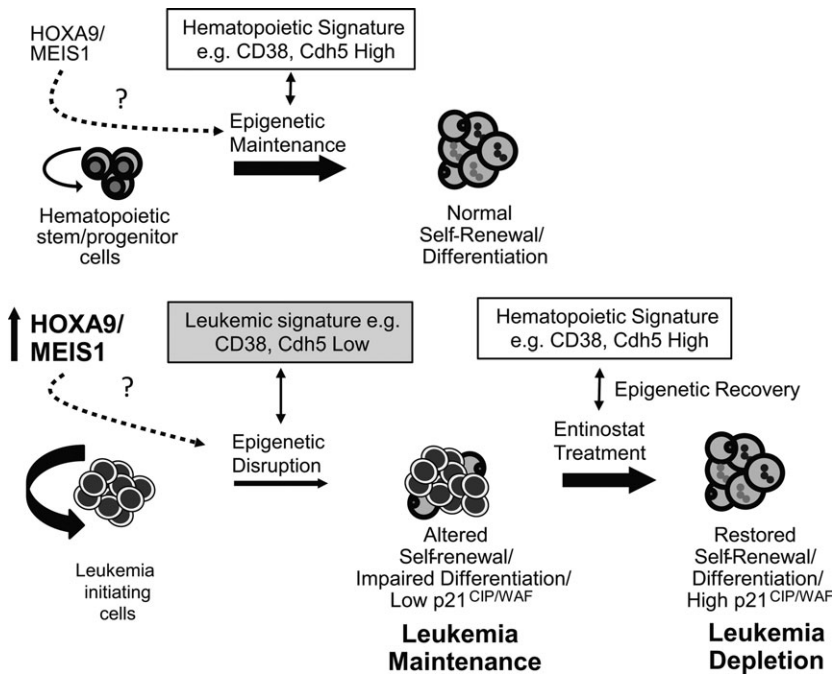

Figure 6. Proposed mechanism of action for Entinostat in A9M leukemia. Hematopoietic development is in balance, with genetic input (*HOXA9/MEIS1*) and epigenetic maintenance, allowing normal differentiation and apoptosis (upper section). Increased *HOXA9/MEIS1* input with potential and associated epigenetic disruption leads to increased proliferation/self-renewal and impaired differentiation. This culminates in leukemia initiation and maintenance. However, maintenance is disrupted by histone deacetylase class I inhibitor (Entinostat) treatment allowing for epigenetic recovery, reduced proliferation/self-renewal, and restored differentiation which results in loss of leukemia maintenance (lower section).

liquid culture. Additionally, A9M-L2 leukemia cells treated with Entinostat demonstrated reduced numbers, size, and metabolism of clonogenic progenitors compared to controls or Panobinostat-treated cells. The differential cellular effects of two HDACis used at concentrations that attain comparable levels of Histone acetylation emphasizes the complexity of epigenetic regulation and warrants further study.

The decrease in colony formation following Entinostat treatment correlated with a dramatic reduction in leukemia initiating cells compared to Panobinostat, control, or vehicle-treated A9M-L2 cells. This clearly demonstrates that A9M-L2 leukemia cells are sensitive to short-term exposure of Entinostat that results in significant depletion and potential purging of the leukemia-initiating cell possibly by a mechanism of reduced proliferation/self-renewal and increased differentiation, in part due to the increased activity of $p21^{CIP/WAF}$ (Fig. 6). Association between HOX/TALE activation and epigenetic drivers such as CBP/P300 recruitment, histone acetylation, and alternative recruitment of RNA polymerase II has recently been reported [41, 42]. Together with the data presented herein, this suggests that collaborating oncogenic dysfunction may result in epigenetic disruption that is potentially targetable therapeutically. Congruent with this, a single treatment of Entinostat, to developing A9M-L2 leukemia, resulted in significant extension in survival (~8 days) compared to control or vehicle-treated mouse recipients. The lack of general cytotoxicity of Entinostat, as demonstrated by it being well-tolerated in NBM cells and failing to impair homing or short-term repopulation, indicates good efficacy which may be of particular value in combination therapies.

Summary

Together these data show that application of sscMap to genetically defined models can identify small molecule inhibitors across species that may be clinically relevant. The ex vivo purging of leukemia maintenance cells and prolonged survival in vivo supports the potential of Entinostat as a therapeutic for *HOXA9* and *MEIS1* overexpressing leukemias. Whether Entinostat has a direct effect on the proto-oncogenes as recently suggested [43] or indirectly through other mechanisms, in CN-AML, remains to be determined. Entinostat prolonged survival in leukemic mice as a single-agent to a similar level as that reported for continuous infusion of a potent small molecule inhibitor [44]. However, epigenetic priming agents, such as HDACis and hypomethylating molecules will most likely be more effective as part of a combined therapeutic approach in leukemia and cancer [45–47]. HDACis are associated with several modes of antitumor activity including modulation of the immune response [48], cell cycle arrest, promotion of differentiation, senescence, and apoptosis [46]. Harnessing the beneficial properties of such compounds while limiting cytotoxic effects will improve their future use particularly in combination therapy.

Advanced connectivity maps, obtained from in vivo studies, may accelerate drug development and redeployment of approved small molecule inhibitors. Therefore, the generation and treatment of clinically relevant in vivo models becomes more pressing. This study demonstrates that the HDAC class I inhibitor Entinostat inhibits disease maintenance and prolongs survival in a clinically relevant murine model of cytogenetically normal AML.

Acknowledgments

We gratefully acknowledge Danielle Gagne, Melanie Fréchette, and Jodie Hay for technical support, as well as the staff within the Biological Resource Unit, Bioinformatics, and Flow Cytometry Cores, Queen's University Belfast. A.T. is a recipient of The American Cancer Society for Beginning Investigator Fellowship from the UICC and supported by Leukemia Lymphoma Research (U.K.) grant numbers 09035 and 07016 and the Northern Ireland Leukemia Research Fund (NILRF). G.D. and L.K. were supported by Leukemia Lymphoma Research (U.K.); G.D. is a recipient of a UICC Fellowship (YY); T.R.L. and K.I.M. were both funded by NILRF, J.M.R. was funded by the Northern Ireland Department of Education and Learning. S.D.Z. was supported by the Biotechnology and Biological Sciences Research Council (BBSRC, U.K.) grant BB/I009051/1. G.S. is a recipient of a Canada Research Chair in molecular genetics of stem cells and is supported by grants from the National Cancer Institute of Canada with funds from the Canadian Cancer Society.

Disclosure of Potential Conflicts of Interest

The authors indicate no potential conflicts of interest.

References

1 Haferlach T, Bacher U, Kohlmann A et al. Discussion of the applicability of microarrays: Profiling of leukemias. Methods Mol Biol 2009;509:15–33.

2 Ross ME, Mahfouz R, Onciu M et al. Gene expression profiling of pediatric acute myelogenous leukemia. Blood 2004;104:3679–3687.

3 Ross ME, Zhou X, Song G et al. Classification of pediatric acute lymphoblastic leukemia by gene expression profiling. Blood 2003;102: 2951–2959.

4 Wouters BJ, Lowenberg B, Delwel R. A decade of genome-wide gene expression profiling in acute myeloid leukemia: Flashback and prospects. Blood 2009;113:291–298.

5 Yeoh EJ, Ross ME, Shurtleff SA et al. Classification, subtype discovery, and prediction of outcome in pediatric acute lymphoblastic leukemia by gene expression profiling. Cancer Cell 2002;1:133–143.

6 Kohlmann A, Grossmann V, Haferlach T. Integration of next-generation sequencing into clinical practice: Are we there yet? Semin Oncol 2012;39:26–36.

7 Lamb J, Crawford ED, Peck D et al. The Connectivity Map: Using gene-expression signatures to connect small molecules, genes, and disease. Science 2006;313:1929–1935.

8 Zhang SD, Gant TW. sscMap: An extensible Java application for connecting small-molecule drugs using gene-expression signatures. Bmc Bioinformatics 2009;10:236.

9 McArt DG, Zhang SD. Identification of candidate small-molecule therapeutics to cancer by gene-signature perturbation in connectivity mapping. Plos One 2011;6:e16382.

10 Zuber J, Radtke I, Pardee TS et al. Mouse models of human AML accurately predict chemotherapy response. Genes Dev 2009;23: 877–889.

11 Zeisig BB, Garcia-Cuellar MP, Winkler TH et al. The oncoprotein MLL-ENL disturbs hematopoietic lineage determination and transforms a biphenotypic lymphoid/myeloid cell. Oncogene 2003;22: 1629–1637.

12 Cuenco GM, Nucifora G, Ren R. Human AML1/MDS1/EVI1 fusion protein induces an acute myelogenous leukemia (AML) in mice: A model for human AML. Proc Natl Acad Sci USA 2000;97:1760–1765.

13 Cuenco GM, Ren R. Cooperation of BCR-ABL and AML1/MDS1/EVI1 in blocking myeloid differentiation and rapid induction of an acute myelogenous leukemia. Oncogene 2001;20:8236–8248.

14 Argiropoulos B, Humphries RK. Hox genes in hematopoiesis and leukemogenesis. Oncogene 2007;26:6766–6776.
15 Lawrence HJ, Rozenfeld S, Cruz C et al. Frequent co-expression of the HOXA9 and MEIS1 homeobox genes in human myeloid leukemias. Leukemia 1999;13:1993–1999.
16 Soulier J, Clappier E, Cayuela JM et al. HOXA genes are included in genetic and biologic networks defining human acute T-cell leukemia (T-ALL). Blood 2005;106:274–286.
17 Golub TR, Slonim DK, Tamayo P et al. Molecular classification of cancer: Class discovery and class prediction by gene expression monitoring. Science 1999;286:531–537.
18 Armstrong SA, Staunton JE, Silverman LB et al. MLL translocations specify a distinct gene expression profile that distinguishes a unique leukemia. Nat Genet 2002;30:41–47.
19 Ferrando AA, Armstrong SA, Neuberg DS et al. Gene expression signatures in MLL-rearranged T-lineage and B-precursor acute leukemias: Dominance of HOX dysregulation. Blood 2003;102:262–268.
20 So CW, Karsunky H, Wong P et al. Leukemic transformation of hematopoietic progenitors by MLL-GAS7 in the absence of Hoxa7 or Hoxa9. Blood 2004;103:3192–3199.
21 Somervaille TC, Matheny CJ, Spencer GJ et al. Hierarchical maintenance of MLL myeloid leukemia stem cells employs a transcriptional program shared with embryonic rather than adult stem cells. Cell Stem Cell 2009;4:129–140.
22 Wong P, Iwasaki M, Somervaille TC et al. Meis1 is an essential and rate-limiting regulator of MLL leukemia stem cell potential. Genes Dev 2007;21:2762–2774.
23 Faber J, Krivtsov AV, Stubbs MC et al. HOXA9 is required for survival in human MLL-rearranged acute leukemias. Blood 2009;113: 2375–2385.
24 Haferlach C, Mecucci C, Schnittger S et al. AML with mutated NPM1 carrying a normal or aberrant karyotype show overlapping biologic, pathologic, immunophenotypic, and prognostic features. Blood 2009;114:3024–32.
25 Kroon E, Krosl J, Thorsteinsdottir U et al. Hoxa9 transforms primary bone marrow cells through specific collaboration with Meis1a but not Pbx1b. EMBO J 1998;17:3714–3725.
26 Wilhelm BT, Briau M, Austin P et al. RNA-seq analysis of 2 closely related leukemia clones that differ in their self-renewal capacity. Blood 2011;117:e27–38.
27 Haferlach T, Kohlmann A, Wieczorek L et al. Clinical utility of microarray-based gene expression profiling in the diagnosis and subclassification of leukemia: Report from the International Microarray Innovations in Leukemia Study Group. J Clin Oncol 2010;28: 2529–2537.
28 Thorsteinsdottir U, Mamo A, Kroon E et al. Overexpression of the myeloid leukemia-associated Hoxa9 gene in bone marrow cells induces stem cell expansion. Blood 2002;99:121–129.
29 Bijl J, Sauvageau M, Thompson A et al. High incidence of proviral integrations in the Hoxa locus in a new model of E2a-PBX1-induced B-cell leukemia. Genes Dev 2005;19:224–233.
30 Thompson A, Quinn MF, Grimwade D et al. Global down-regulation of HOX gene expression in PML-RARalpha + acute promyelocytic leukemia identified by small-array real-time PCR. Blood 2003;101: 1558–1565.
31 Hu E, Dul E, Sung CM et al. Identification of novel isoform-selective inhibitors within class I histone deacetylases. J Pharmacol Exp Ther 2003:720–728.
32 Ocio EM, Vilanova D, Atadja P et al. In vitro and in vivo rationale for the triple combination of panobinostat (LBH589) and dexamethasone with either bortezomib or lenalidomide in multiple myeloma. Haematologica 2010;95:794–803.
33 Srivastava RK, Kurzrock R, Shankar S. MS-275 sensitizes TRAIL-resistant breast cancer cells, inhibits angiogenesis and metastasis, and reverses epithelial–mesenchymal transition in vivo. Mol Cancer Ther 2010;9:3254–3266.
34 Hooker JM, Kim SW, Alexoff D et al. Histone deacetylase inhibitor, MS-275, exhibits poor brain penetration: Pk studies of [C]MS-275 using positron emission tomography. ACS Chem Neurosci 2010;1: 65–73.
35 Standeven AM, Johnson AT, Escobar M et al. Specific antagonist of retinoid toxicity in mice. Toxicol Appl Pharmacol 1996;138:169–175.
36 Schwind S, Marcucci G, Maharry K et al. BAALC and ERG expression levels are associated with outcome and distinct gene and microRNA expression profiles in older patients with de novo cytogenetically normal acute myeloid leukemia: A Cancer and Leukemia Group B study. Blood 2010;116:5660–5669.
37 Becker H, Marcucci G, Maharry K et al. Favorable prognostic impact of NPM1 mutations in older patients with cytogenetically normal de novo acute myeloid leukemia and associated gene- and microRNA-expression signatures: A Cancer and Leukemia Group B study. J Clin Oncol 2010;28:596–604.
38 Muntean AG, Hess JL. The pathogenesis of mixed-lineage leukemia. Annu Rev Pathol 2012;7:283–301.
39 Huang Y, Sitwala K, Bronstein J et al. Identification and characterization of Hoxa9 binding sites in hematopoietic cells. Blood 2012;119: 388–398.
40 Rosato RR, Almenara JA, Grant S. The histone deacetylase inhibitor MS-275 promotes differentiation or apoptosis in human leukemia cells through a process regulated by generation of reactive oxygen species and induction of p21CIP1/WAF1 1. Cancer Res 2003;63:3637–3645.
41 Scandura JM, Roboz GJ, Moh M et al. Phase 1 study of epigenetic priming with decitabine prior to standard induction chemotherapy for patients with AML. Blood 2011;118:1472–1480.
42 Dassé E, Volpe G, Walton DS et al. Distinct regulation of c-myb gene expression by HoxA9, Meis1 and Pbx proteins in normal hematopoietic progenitors and transformed myeloid cells. Blood Cancer J. 2012; 2:e76.
43 Stumpel DJ, Schneider P, Seslija L et al. Connectivity mapping identifies HDAC inhibitors for the treatment of t(4;11)-positive infant acute lymphoblastic leukemia. Leukemia 2012;26:682–692.
44 Daigle SR, Olhava EJ, Therkelsen CA et al. Selective killing of mixed lineage leukemia cells by a potent small-molecule DOT1L inhibitor. Cancer Cell 2011;20:53–65.
45 Huang Y, Sitwala K, Bronstein J et al. Identification and characterization of Hoxa9 binding sites in hematopoietic cells. Blood 2012:12; 119:388–98.
46 Lane AA, Chabner BA. Histone deacetylase inhibitors in cancer therapy. J Clin Oncol 2009;27:5459–5468.
47 Bhatla T, Wang J, Morrison DJ et al. Epigenetic reprogramming reverses the relapse-specific gene expression signature and restores chemosensitivity in childhood B-lymphoblastic leukemia. Blood 2012; 119:5201–5210.
48 Glauben R, Sonnenberg E, Zeitz, et al. HDAC inhibitors in models of inflammation-related tumorigenesis. Cancer Lett 2009;280:154–159.

See www.StemCells.com for supporting information available online.